

# Structural Elucidation of Magnetic Biochar Derived from Recycled Paper Waste Sludge

Masale C. Manoko<sup>a,\*</sup>, Evans M.N. Chirwa<sup>a</sup>, Katlego Makgopa<sup>b</sup>

<sup>a</sup> Department of Chemical Engineering, University of Pretoria, Pretoria, 0002, South Africa

<sup>b</sup> Department of Chemistry, Faculty of Science, Tshwane University of Technology, 175 Nelson Mandela Drive, Arcadia, Pretoria 0002, South Africa  
 Mmanoko@gmail.com

Partially treated wastewater released into natural water bodies leads to eutrophication which poses a threat to aquatic animals and water supply security. The recovery of nutrients from wastewater, and their subsequent recycling in other agricultural applications contribute to nutrient recycling and utilization. Biochar derived from biomass waste is increasingly seen as a multifunctional material for the adsorption of various pollutants from wastewater. This is due to its low production cost and carbon footprint. Recycled paper waste sludge (RPWS) is another abundant type of woody biomass that yields biochar as a by-product during pyrolysis processes. This material has emerged as a feedstock to produce several liquid fuels such as bio-oils and alcohols. However, there has been little application of the material as an adsorbent for the removal of nutrients and pollutants from wastewater. Two variants of RPWS were available for this work, primary sludge from screening processes and secondary sludge from a clarification plant were used as feedstocks to produce biochar products via slow pyrolysis at 550 °C, and 650 °C. Furthermore, a step to produce magnetic biochar was added through impregnation with Fe<sup>3+</sup> and Fe<sup>2+</sup> and subsequent co-pyrolysis. The biochar yields are promising for the pyrolysis of RPWS. The structural analysis and morphological characterization of the samples (before and after pyrolysis) were done through thermogravimetric analysis (TGA), Scanning Electron Microscopy (SEM-EDS), Fourier Transform Infrared Spectroscopy (FTIR), X-ray diffraction (XRD), and Brunauer-Emmet Teller (BET). The residues after pyrolysis showed good physical and chemical qualities that can be beneficial for the adsorption of nutrients in wastewater treatment.

## 1. Introduction

The discharge of partially treated wastewater increases the phosphorus and nitrogenous compounds in receiving water bodies causing excessive vegetation growth and algal blooms leading to eutrophication (Hasan et al., 2021). Consequently threatens water security, aquatic ecosystems, and human health (Nguyen et al., 2021). The development of cost-effective solutions to recover these nutrients from wastewater and apply them in beneficial areas or sectors is of great importance as the world strives for a circular economy.

There are numerous methods applied in the removal or recovery of nutrients from wastewater such as biological nitrification-denitrification process (BNR), ion-exchange, air stripping, struvite chemical precipitation, and adsorption, however, each process has limitations with BNR requiring large facilities and longer residence times and the other processes except for adsorption producing waste streams which still need to be disposed of safely increasing their operational costs (Hasan et al., 2021). Several adsorbents such as zeolites, polymeric adsorbents, clay minerals, porous silica, biochar, and activated carbon have been used in the removal or recovery of nutrients from wastewater, with activated carbon having the widest application (Almanassra et al., 2021). However, activated carbon's limitation is very weak surface charged groups which translate into poor adsorption of anions like phosphates (Miyazato et al., 2020).

Since Chen et al. (2011) developed magnetic biochar derived from biomass to adsorb nutrients from wastewater, many researchers have studied the removal efficiency of biochars from a variety of feedstocks in removing various pollutants from wastewater. Biochar is a product of pyrolysis, which is the heating of biomass

at elevated temperatures in an inert environment (Yaashikaa et al., 2020), magnetizing biochars increases their affinity for nutrients like phosphorus and allows easy separation from wastewater using magnets. This process provides a suitable alternative to biomass waste management practices such as landfilling, land application, and incineration which can potentially pollute the receiving environment. Slow pyrolysis/carbonization of biomass is preferred when biochar is the desired product; the quality of biochar produced is dependent on feedstock and conditions such as carbonization temperature, moisture, and residence time (Basu, 2018).

A lot of focus in the literature has been on the development of biochar using agricultural waste than sludge from industrial applications like fibre recycling. Biochar has demonstrated nutrients adsorption results similar or higher than that of commercial adsorbents (Devi and Saroha, 2015). To understand the potential of paper waste sludge-derived biochar, its physicochemical properties and morphology need to be studied in detail. The feedstock, elemental composition, and carbonization parameters have a major effect on the desired biochar quality and quantity, thus require careful management (Yaashikaa et al., 2020). These conditions coupled with the synthesis of biochar either through activation or magnetization before or after carbonization are areas still being researched across a wide variety of biomass sources. In this study, paper waste sludge-derived biochar and a magnetic derivative were produced in the temperature range of 550-650 °C and characterized to assess their viability as alternatives to the current expensive adsorbents used in wastewater treatment.

## 2. Materials and methods

### 2.1 Feedstock collection and chemicals

The two variants of RPWS, raw (RPS) collected from pulp screening and secondary (SPS) collected from clarification plant were collected from Mpact Recycled fibre Springs Mill, in East Johannesburg, South Africa. Analytical grade ferric chloride hexahydrate ( $\text{FeCl}_3 \cdot 6\text{H}_2\text{O}$ ), ferrous chloride ( $\text{FeCl}_2 \cdot 4\text{H}_2\text{O}$ ) were sourced from Glassworld & chemical suppliers. Nitrogen gas was sourced from Afrox and deionized water was produced from an Elga Veolia water purification system LA759.

### 2.2 Biochar preparation

The sludge underwent a natural drying process at approximately 27 °C onsite at the Mill in a drying area for 10 days. The samples were milled, homogenized, and filled into four 2L ceramic pots with no space left, sealed with a lid, and numbered. Each pot contained  $680 \pm 2$  g SPS and  $600 \pm 2$  g RPS feedstock. During the preparation of magnetic biochar with magnetite nanoparticles serving as the magnetic medium, a 1,000 mL solution of 1:1 molar ratio ferric chloride and ferrous chloride was prepared and mixed with the two variants of prepared paper waste sludge under rigorous mechanical stirring similar to the method reported by (Chen et al., 2011), the stirring continued for 0.5 h. The samples were then filled into numbered ceramic pots with no space left and sealed with lids. Both pristine and impregnated samples were oven-dried for 24 h at  $110 \pm 2$  °C before carbonization at 550 °C and 650 °C. Carbonization was performed in a muffle furnace equipped with a digital temperature controller (RKC RB 100, Japan) under 99 % purity nitrogen  $\text{N}_2$  purge with a heating rate of 5 °C/min and 1 h residence time, the samples were then cooled to room temperature before being taken out and denoted RPSX, SPSX, MBC-RPSX and MBC-SPSX with MBC denoting Magnetic biochar and X the corresponding carbonization temperature. All the experiments were conducted in triplicate and average results are presented.

### 2.3 Biochar yield

Yield can be determined as the ratio of the produced biochar to the initial mass of RPWS subjected to carbonization (Sahoo et al, 2021).

$$\text{Biochar Yield} = \frac{\text{Mass of biochar}}{\text{Mass of PWS}} \times 100 \quad (1)$$

### 2.4 Characterization

RPWS and biochar samples were characterized to analyse the impregnation and carbonization temperature effect on the morphological, chemical, and functional characteristics. Thermogravimetric analysis (TGA) of both samples was performed using a Hitachi STA7300 TGA-DTA following the ASTM D7582 – 15 method (Sangsuk et al., 2020) to identify moisture, volatile matter (VM), ash, and fixed carbon (FC). Fixed carbon was calculated by difference [Original Sample weight – (Moisture + Volatiles + Ash)].

Elemental analysis was performed using a Flash 2000 CHNS Elemental analyser from ThermoFisher Scientific, BET analysis was performed using a Micromeritics Tri-Star II surface area and porosity instrument, the surface functional groups were analysed using a Perkin Elmer 100 Spectrophotometer where FTIR Spectra were recorded in the region of 500 – 4000  $\text{cm}^{-1}$ , XRD was analysed using a PANalytical X'Pert Pro powder diffractometer, XRF analysis was performed using a Thermo Fisher ARL Perform'X Sequential XRF instrument

with Uniquant software, SEM was conducted using a Zeiss Crossbeam 540 FEG scanning electron microscope at 2kv. EDS-Elemental Mapping was conducted using a Zeiss Ultra FEG scanning electron microscope with oxford instruments Aztec 3.0 SP1 software.

### 3. Results and discussion

#### 3.1 Biochar yield

The biochar yield from the two sludge variants of pristine and synthesized feedstock are shown in Table 1, an increase in carbonization temperatures results in lower biochar yield (Hernandez-Mena et al., 2014). RPS biochar yields were lower than SPS biochars by 20.40 % at 550 °C and 19.19 % at 650 °C due to greater losses of volatile components during dehydration of hydroxyl groups and the degradation of cellulose, hemicellulose, and lignin as temperature increased. Findings comparable to (Ridout et al., 2016) with cellulose, hemicellulose, lignin, and extractives compositions (db wt. %) of 49.5, 19, 20.5 and 10.5.

Table 1: Carbonization yield (weight percentage)

Sample Name	550 °C (% d.b)	650 °C (% d.b)
SPS	45.65	41.78
RPS	25.20	21.93
MBC-SPS	46.89	41.04
MBC-RPS	26.54	22.50

#### 3.2 Proximate and ultimate analysis

Proximate and ultimate analysis results are shown in Table 2. RPS contains more volatiles and SPS ash content is significantly higher than RPS due to the presence of fillers and coatings used in board manufacturing. The elemental composition of the raw samples is within the range of previous findings from similar feedstock (Sotoudehnia et al., 2020).

Table 2: Proximate & Elemental Analysis of RPS and SPS (weight percentage, dry basis)

Sample Name	Moisture	Volatile Matter	Fixed Carbon	Ash	C	H	O <sup>a</sup>	N	S
RPS	12.67	73.53	9.31	4.69	46.06	5.84	47.91	0.06	0.13
SPS	5.44	54.47	5.82	34.51	41.06	4.41	54.17	0.24	0.12

a - Determined by the difference

#### 3.3 Brunauer, Emmett, and Teller (BET) surface area

A correlation of the surface area and carbonization temperature was conducted and the BET results are shown in Table 3. It can be noticed that an increase in carbonization temperature translated into an increase in surface area due to the progressive destruction of aliphatic alkyl and ester functional groups (Devi and Saroha, 2015). RPS surface area increase with temperature is significantly higher than that of SPS due to devolatilization which encourages pore formation. The synthesised biochars' surface area was significantly lower than the pristine biochars due to the magnetite and CaCl<sub>3</sub> coating the surface of the chars and the resultant pores.

Table 3: Raw sample and biochar BET Surface area results

Sample	Raw Sample	550 °C (m <sup>2</sup> /g)	650 °C (m <sup>2</sup> /g)
SPS	1.42	31.89	109.64
RPS	0.19	21.67	135.28
MBC-SPS	-	9.67	55.17
MBC-RPS	-	18.41	76.81

#### 3.4 X-Ray Fluorescence (XRF)

The XRF results indicated the presence of clay and calcium carbonate in the feedstocks and subsequent biochars. This is primarily due to the usage of fillers and coating agents such as kaolin Al<sub>2</sub>Si<sub>2</sub>O<sub>5</sub>(OH)<sub>4</sub>, titanium dioxide TiO<sub>2</sub>, and Calcium carbonate CaCO<sub>3</sub>, during recycled board production.

Table 4: Raw sample and biochar XRF results

Sample	SiO <sub>2</sub>	Al <sub>2</sub> O <sub>3</sub>	MgO	Na <sub>2</sub> O	Fe <sub>2</sub> O <sub>3</sub>	TiO <sub>2</sub>	CaO	P <sub>2</sub> O <sub>5</sub>	SO <sub>3</sub>	K <sub>2</sub> O	LOI	Total
SPS	18.64	9.93	4.90	0.37	0.92	2.62	11.62	0.21	0.56	0.16	49.04	99.00
RPS	18.21	8.52	0.61	0.05	1.28	2.93	11.00	0.14	0.32	0.16	56.38	99.60
RPS 550	13.59	6.24	2.56	0.09	0.55	1.13	6.85	0.11	0.01	0.03	68.34	99.50
MBC-RPS 550	7.04	2.94	1.32	0.15	19.68	0.73	1.92	0.06	-	0.04	66.01	99.89
SPS 650	19.18	15.3	1.53	0.1	0.76	1.79	16.55	0.17	0.04	0.04	44.24	99.70
MBC-SPS 650	12.14	9.79	0.90	0.07	12.46	1.15	11.10	0.11	0.04	0.01	52.13	99.90

### 3.5 X-Ray Diffraction (XRD)

The structure and phase purity of the feedstock and biochars were investigated by XRD and shown in Figure 1. Biochar showed characteristics of cellulose and amorphous nature, the peak at 11 ° was defined as Talc, with its intensity increasing in the pristine biochar and reducing significantly in the synthesized biochar, the peak intensity increases as dehydration occurs again. Kaolinite peaks at 14-14.5, 26-29 ° disappears after 550 °C as it decomposes into amorphous metakaolinite (Varga, 2007). Calcite peaks at 34, 46, and 50.5-52.5 ° were identified and their intensity increased with temperature due to the decomposition of CaCO<sub>3</sub>, their intensity disappears in the synthesized chars due to CaCO<sub>3</sub> dissolving and forming amorphous CaCl<sub>3</sub> during impregnation. The sharp strong peaks at 35, 37-38.5, 42 ° were identified as those of well-crystallized magnetite.

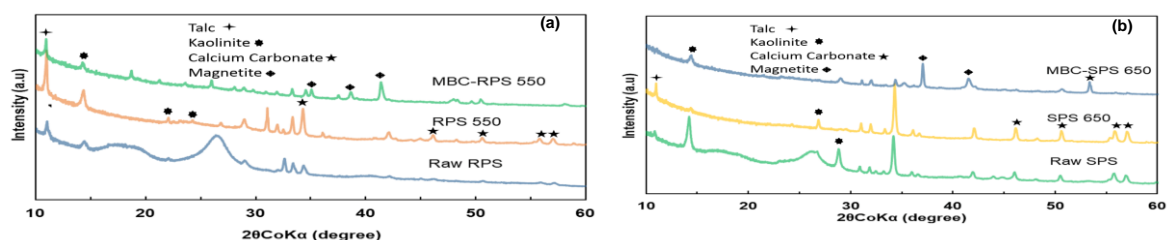


Figure 1: XRD patterns for RPWS, pristine and synthesized biochar from RPS (a) and SPS (b)

### 3.6 FTIR

The bands produced from FTIR analysis of both samples and their resultant biochars are typical biomass-derived biochar and Iron oxide (Chen et al., 2011) as shown in Figure 2. The observed decrease of bands between 3,200 and 3,600 cm<sup>-1</sup> is due to the loss of hydroxyl (OH<sup>-</sup>) functional groups as temperature increases, further adsorption studies to reveal the effect of (OH<sup>-</sup>) loss. The peaks at 1010, 1020, 1100, and 1110 cm<sup>-1</sup> were attributed to C-O-C bonds (Méndez et al, 2009). Calcium carbonate presence is indicated by both narrow 870 and wide 1,410 cm<sup>-1</sup> peaks. The peaks disappear in the impregnated MBC-denoted biochars due to the dissolution of CaCO<sub>3</sub> and the formation of calcium chloride CaCl<sub>3</sub> during the impregnation of the raw samples. The band at 1,600 cm<sup>-1</sup> is attributed to kaolinite in the samples and is consistent with XRF analysis and XRD plots above in 3.4 and 3.5. The peak at 1,600 is attributed to C=C bonds in carboxylic acids.

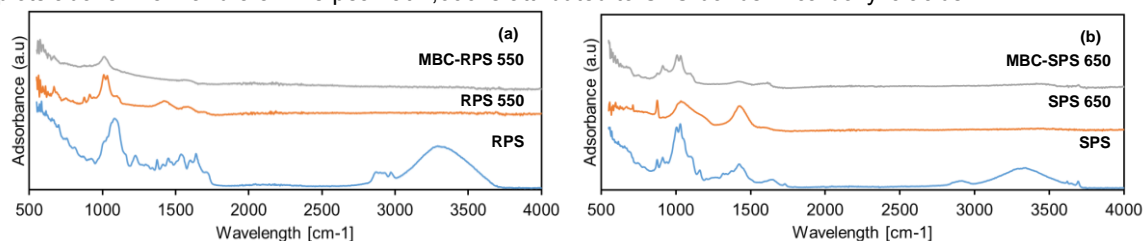


Figure 2: FTIR bands for RPWS, pristine and synthesized biochar from RPS (a) and SPS (b)

### 3.7 Scanning Electron Microscopy (SEM)

Figure 3 shows the fibrous morphology of feedstock, pristine, and synthesized biochar from the different carbonization temperatures, SPS is flaky with fibres protruding from bulk flakes of clays, and RPS is composed of mainly of tangled fibres with minimal clays which is consistent with XRD and XRF findings. Pore development is seen to increase with carbonizing temperatures due to devolatilization and hydroxyl group loss which is

confirmed by FTIR. The synthesized samples exhibit a structure similar to the pristine biochar with the only difference being that they are coated with nanoparticles attached to the surface and within the developed pores.

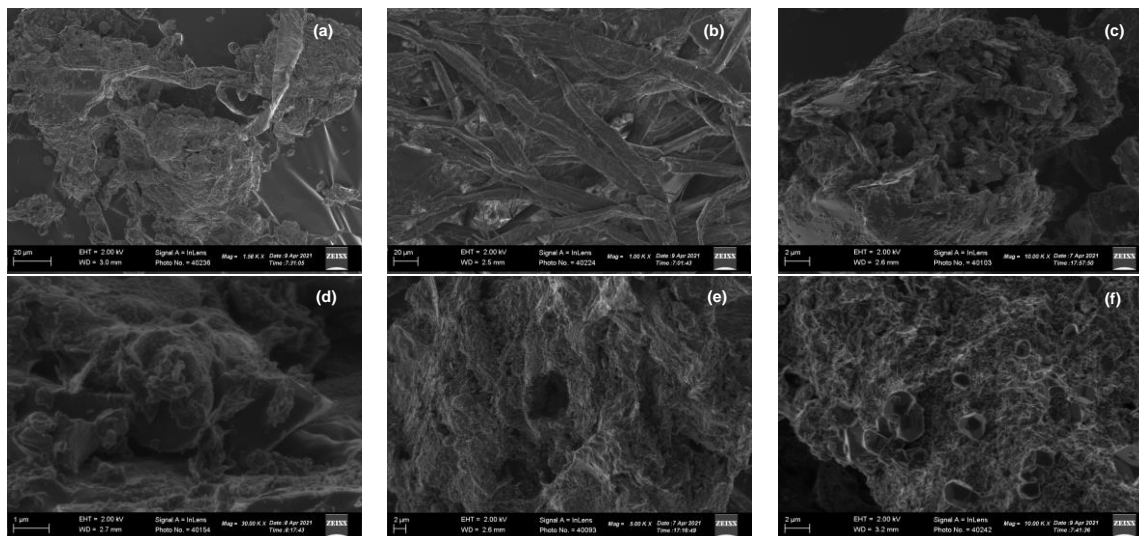


Figure 3: SEM images of SPS (a), RPS (b), RPS 550 (c), MBC-RPS 550 (d), SPS 550 (e) & (f) MBC-SPS 550

### 3.8 Energy Dispersive X-Ray Spectroscopy (EDS) and elemental mapping

The elemental composition of the raw samples, pristine and synthesized biochars are shown in Table 5, it is evident that calcium carbonate, titanium dioxide  $TiO_2$ , and kaolin  $Al_2Si_2O_5(OH)_4$  are the dominantly used fillers and coating agents during board production due to the presence of their oxides after carbonization. The electron mapping is consistent with SEM micrographs on the presence of magnetite nanoparticles on the surface of the synthesized biochar, clear deposits can be seen consistently on the synthesized biochars as per Figure 3 amorphous  $CaCl_2$  is also observed coating the biochars, consistent with the x-ray analysis.

Table 5: Elemental analysis (weight percentage)

Sample	O (% d.b)	Mg (% d.b)	Al (% d.b)	Si (% d.b)	Ca (% d.b)	Fe (% d.b)	Cl (% d.b)	Ti (% d.b)
SPS	47.29	0.43	12.16	13.40	22.51	1.18	0.16	2.87
RPS	44.93	9.23	7.17	10.60	26.32	3.89	0.89	2.97
RPS 550	66.81	1.17	4.83	6.57	16.00	2.20	1.25	1.17
MBC-RPS 550	28.14	0.90	2.52	2.69	2.55	39.57	23.27	1.59
SPS 650	49.60	0.88	10.71	11.67	22.19	1.31	1.20	2.44
MBC-SPS 650	41.12	0.45	5.01	5.08	12.28	13.36	17.16	0.95

The electron mapping is consistent with SEM micrographs on the presence of magnetite nanoparticles on the surface of the synthesized biochar, clear deposits can be seen consistently on the synthesized biochars as per Figure 4 amorphous  $CaCl_2$  is also observed coating the biochars, consistent with XRF results.

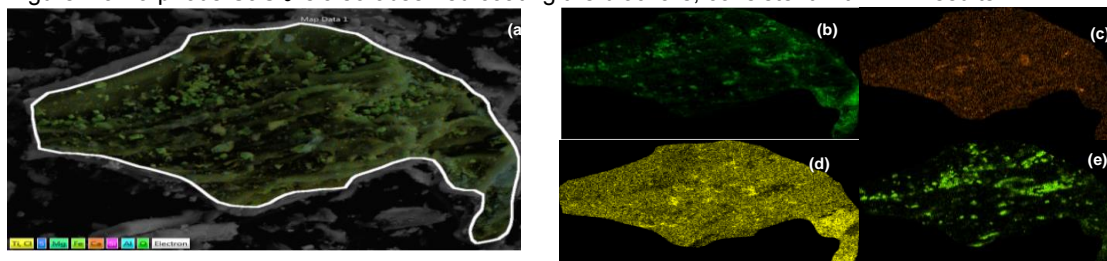


Figure 4: EDS elemental Mapping of synthesized biochar particle, (a) Particle Map (b) O, (c) Ca (d) Cl, (e) Fe

#### 4. Conclusions

The carbonization of RPWS yields acceptable biochar, with RPS yields reduced significantly as temperature increased. Careful carbonization condition considerations must be made when biochar is the target from RPS for sufficient yields. The filler and coating agent characteristics of the feedstock add properties that can be beneficial in the removal of nutrients during wastewater treatment such as phosphates and nitrates due to the formation of oxides. The successfully magnetized biochar would also improve the absorption of the nutrients due to the magnetite's high affinity for them. The valorisation of RPWS into Pristine and magnetic biochar produces a potential low-cost adsorbent and negates the Mill waste disposal burden. Adsorption studies are recommended to assess the efficacy of RPWS biochars during wastewater treatment.

#### References

- Almanassra I.W., McKay G., Kochkodan V., Ali Atieh M., Al-Ansari T., 2021, A state of the art review on phosphate removal from water by biochars, *Chemical Engineering Journal*, 409,128211.
- Basu P., 2018, *Biomass Gasification, Pyrolysis and Torrefaction: Practical Design and Theory*, Elsevier Science & Technology, San Diego, United States.
- Chen B., Chen Z., Lv S., 2011, A novel magnetic biochar efficiently sorbs organic pollutants and phosphate, *Bioresource Technology*, 102(2), 716-723.
- Devi P., Saroha A.K., 2015, Effect of pyrolysis temperature on polycyclic aromatic hydrocarbons toxicity and sorption behaviour of biochars prepared by pyrolysis of paper mill effluent treatment plant sludge, *Bioresource Technology*, 192, 312-320.
- Hasan M.N., Altaf M.M., Khan N.A., Khan A.H., Khan A.A., Ahmed S., Kumar P.S., Naushad M., Rajapaksha A.U., Iqbal J., Tirth V., Islam S., 2021, Recent technologies for nutrient removal and recovery from wastewaters: A review, *Chemosphere*, 277,130328.
- Hernandez-Mena L.E., Pécoraa A., Beraldob A.L., 2014, Slow pyrolysis of bamboo biomass: analysis of biochar properties, *Chemical Engineering Transactions*, 37, 115-120.
- Méndez A., Fidalgo J.M., Guerrero F., Gascó G., 2009, Characterization and pyrolysis behaviour of different paper mill waste materials, *Journal of Analytical and Applied Pyrolysis*, 86(1), 66-73.
- Miyazato T., Nuryono N., Kobune M., Rusdiarso B., Otomo R., and Kamiya Y, 2020, Phosphate recovery from an aqueous solution through adsorption-desorption cycle over thermally treated activated carbon, *Journal of Water Process Engineering*, 36,101302.
- Nguyen L.H., Van H.T., Chu T.H.H., Nguyen T.H.V., Nguyen T.D., Hoang L.P., Hoang V.H., 2020, Paper waste sludge-derived hydrochar modified by iron (III) chloride for enhancement of ammonium adsorption: An adsorption mechanism study, *Environmental Technology & Innovation*, 21,101223.
- Ridout A.J., Carrier M., Collard F-X., Görgens J., 2016, Energy conversion assessment of vacuum, slow and fast pyrolysis processes for low and high ash paper waste sludge, *Energy Conversion and Management*, 111,103114.
- Sahoo S.S., Vijay V.K., Chandra R., Kumar H., 2021, Production and characterization of biochar produced from slow pyrolysis of pigeon pea stalk and bamboo, *Cleaner Engineering and Technology*, 3,100101.
- Sangsuk S., Buathong C., Suebsiri S., 2020, High-energy conversion efficiency of drum kiln with heat distribution pipe for charcoal and biochar production, *Energy for Sustainable Development*, 59, 1-7.
- Sotoudehnia F., Baba Rabiou A., Alayat A., McDonald A.G., 2020, Characterization of bio-oil and biochar from pyrolysis of waste corrugated cardboard, *Journal of Analytical and Applied Pyrolysis*, 145,104722.
- Varga G., 2007, The structure of kaolinite and metakaolinite, *Epitoanyag*, 59(1), 6-9.
- Yaashikaa P.R., Kumar P.S., Varjani S., Saravanan A., 2020, A critical review on the biochar production techniques, characterization, stability and applications for circular bioeconomy, *Biotechnology Reports*, 28, e00570.